

Fundamental physics with the Lyman-alpha forest: constraints on the growth of structure and neutrino masses from SDSS with effective field theory

Mikhail M. Ivanov,^{1,*} Michael W. Toomey,^{1,†} and Naim Göksel Karaçaylı^{2,3,4,‡}

¹*Center for Theoretical Physics, Massachusetts Institute of Technology, Cambridge, MA 02139, USA*

²*Center for Cosmology and AstroParticle Physics, The Ohio State University,
191 West Woodruff Avenue, Columbus, OH 43210, USA*

³*Department of Astronomy, The Ohio State University,
4055 McPherson Laboratory, 140 W 18th Avenue, Columbus, OH 43210, USA*

⁴*Department of Physics, The Ohio State University,
191 West Woodruff Avenue, Columbus, OH 43210, USA*

We present an effective field theory (EFT) approach to extract fundamental cosmological parameters from the Lyman-alpha forest flux fluctuations as an alternative to the standard simulation-based techniques. As a first application, we re-analyze the publicly available one-dimensional Lyman-alpha flux power spectrum data from the Sloan Digital Sky Survey (SDSS). Our analysis relies on informative priors on EFT parameters which we extract from a combination of public hydrodynamic simulation and emulator data. Assuming the concordance cosmological model, our one-parameter analysis yields a 2% measurement of the late time mass fluctuation amplitude $\sigma_8 = 0.841 \pm 0.017$, or equivalently, the structure growth parameter $S_8 = 0.852 \pm 0.017$, consistent with the standard cosmology. Combining our EFT likelihood with Planck + baryon acoustic oscillation data, we find a new constraint on the total neutrino mass, $\sum m_\nu < 0.08$ eV (at 95% CL). Our study defines priorities for the development of EFT methods and sets the benchmark for cosmological analyses of the Lyman-alpha forest data from the Dark Energy Spectroscopic Instrument.

Introduction. The distribution of galaxies and matter on cosmic scales, known as large-scale structure, is a key probe of cosmological physics. In particular, the cosmic web has been instrumental in discoveries and subsequent studies of dark matter and dark energy, thereby helping establish the standard Λ Cold Dark Matter (Λ CDM) model of cosmology. Within Λ CDM, structure formation has a hierarchical pattern: small structures form in the early Universe at high redshifts while larger structures form at later times. Some of the earliest and smallest clustering structures available for observations are neutral hydrogen clouds that fill the intergalactic medium at redshifts $z \gtrsim 2$. These clouds absorb light from distant quasars, creating characteristic combs in their spectra, known as the Lyman-alpha ($\text{Ly}\alpha$) forest [1–9]. Fluctuations in the transmitted flux from quasars trace the underlying dark matter density, providing a probe of fundamental physics at scales of a few Megaparsec and redshifts $2 \lesssim z \lesssim 5$. Thanks to this advantageous property,

the $\text{Ly}\alpha$ forest data have provided an excellent probe of Λ CDM, dark matter, neutrino masses, primordial features, and many other extensions of the concordance model [8–23].

Decades of observational and theoretical efforts in $\text{Ly}\alpha$ forest physics have culminated in percent-level precision measurements of the baryon acoustic oscillations, flux power spectrum (FPS) and three-dimensional correlations of the $\text{Ly}\alpha$ forest flux with the Sloan Digital Sky Survey (SDSS) [14, 24–26], and FPS measurements [27–30] with high-resolution spectrographs such as X-Shooter [31, 32], HIRES [33, 34], and UVES [35, 36]. The number of quasar spectra with the $\text{Ly}\alpha$ forest will soon increase multifold with the ongoing Dark Energy Spectroscopic Instrument (DESI) [37, 38].

With great statistical power comes great responsibility for modeling accuracy. This is particularly important given that the effective slope and amplitude of the linear matter power spectrum inferred from the SDSS 1D FPS are found to be in some tension with the Λ CDM model [16, 23, 25, 39]. To reconcile this potential discrepancy new physics interpretations of this tension have been suggested, e.g. in [23, 39–41]. Given the signifi-

* ivanov99@mit.edu

† mtoomey@mit.edu

‡ karacayli.1@osu.edu

cance of these results, it is imperative to independently test the modeling assumptions behind Ly α forest power spectrum analyses.

The standard approach to the Ly α physics has relied on emulators trained on hydrodynamic simulations [16, 42–48]. These simulations are based on detailed models of underlying astrophysics, e.g. star formation, stellar feedback, reionization. Powerful as they are, these simulations are currently limited by resolution issues. Emulators also face additional uncertainties in the numerical interpolation over a grid of simulations.

In this *Letter*, we explore an alternative approach to the Ly α forest analysis based on ideas borrowed from particle physics. The perturbative or effective field theory (EFT) approaches to large-scale structure develop the description of cosmic web dynamics that is agnostic about the underlying astrophysical processes [49–52] (see [53–61] for perturbative calculations of the Ly α forest). In our context, the only two assumptions that EFT makes are that the flux absorption fluctuations trace the underlying dark matter density and non-linear corrections are perturbative [61]. EFT does not make additional assumptions about gas physics. In particular, it does not impose any temperature-density relation. The relationship between flux fluctuations and the dark matter density field should be described by an analytic function, which can be Taylor expanded on large scales. Then the terms in this Taylor series are parameterized using the fundamental symmetries of the problem, such as the rotations around the line-of-sight direction and the equivalence principle. Perturbative EFT approaches have been especially successful in galaxy clustering analyses, where they have become a standard tool for parameter estimation [62–66]. This *Letter* presents an application of the similar approach to the Ly α data.

An important advantage of EFT is its flexibility: a typical calculation of relevant non-linear corrections to the Ly α power spectrum takes about 1 second [67], which allows one to efficiently explore cosmological models without the need to re-run hydrodynamical simulations for new parameters added. In contrast to emulators, the EFT theory model can be consistently computed for every point in parameter space, thereby removing any uncertainty associated with the grid interpolation. This is especially valuable for extended cosmological models proposed as a resolution to the above tension between Λ CDM and the SDSS Ly α data. A rigorous interpreta-

tion of the Ly α data in the context of such models requires one to self-consistently recompute the FPS, which can be easily done with EFT.

This *Letter* lays the groundwork for systematic full-shape analyses of Ly α data with EFT. Here, we re-analyze the publicly available SDSS data on the 1D FPS using the EFT for Ly α data developed in [61]. Our work can be seen as an extension of earlier efforts to use perturbative techniques for the Ly α forest 1D data analysis [55–57, 59, 60]. The main novelties of our work are formulating a self-consistent theory for Ly α in 3D, and fitting cosmological parameters from Ly α data just like in the full-shape analyses of galaxy surveys.

Our work pursues several goals. First, we develop an efficient toolkit to probe fundamental cosmology with the Ly α forest and test it against the real data. Second, we investigate if the SDSS Ly α data are consistent with Λ CDM within the EFT approach. Third, we identify key directions for the future development of the Ly α EFT full-shape analysis.

Data. Our analysis is based on quasar spectra from the fourteenth data release (DR14) of SDSS [25], which consists of the Baryon Oscillation Spectroscopic Survey (BOSS) and extended-BOSS (eBOSS) samples. The 1D FPS measurements from the SDSS quasars in the redshift range $2.2 < z < 4.6$ are publicly available. In our analysis, we will focus on a more narrow redshift range $3.4 \leq z \leq 4.2$, encompassing 6 redshift bins with centers 3.2, 3.4, 3.6, 3.8, 4.0, 4.2. We do not use the lower redshift bins because their description requires an accurate calibration of the bias parameters that is not possible with publicly available simulations. We discard the highest two redshift bins in this work in order to be more conservative in light of a potential sensitivity to inhomogeneous reionization [68]. To build the power spectrum likelihood, we use the public covariance matrices that include additional diagonal corrections to account for systematic effects due to finite resolution, active galactic nuclei feedback, damped Ly α systems etc. [25].

Theory model overview. Let us start our theory background with a brief discussion of the galaxy clustering in redshift space at the lowest (linear) order in dark matter perturbations [51, 69, 70]. Causality, the equivalence principle, and rotational symmetry imply that on the largest scales, the galaxy overdensity field $\delta_g = n_g/\bar{n}_g - 1$ (n_g being the galaxy number density, and overbar denotes spatial averaging), should be linearly proportional

to the dark matter overdensity $\delta^{(1)}$ computed in linear theory,

$$\delta_g = b_1 \delta^{(1)}. \quad (1)$$

The coefficient of proportionality b_1 is called the linear bias parameter. It encapsulates details of the galaxy formation physics, and its prediction is possible given a galaxy formation model. In EFT, b_1 is treated as a nuisance parameter to marginalize over. Since Eq. (1) is written in the galaxy rest frame, to describe the galaxy distribution seen by the observer $\delta_g^{(s)}$, one has to transform δ_g in Eq. (1) to the observer's frame, which introduces redshift-space distortions [71, 72]. At the linear level, the mapping between the two frames yields

$$\delta_g^{(s)} = b_1 \delta^{(1)} - \frac{\partial_{\parallel} v_{\parallel}^{(1)}}{aH}, \quad (2)$$

where $v_i^{(1)}$ is the peculiar velocity of galaxies, H is the Hubble parameter, a is the metric scale factor, and the subscript \parallel denotes the projection onto the line-of-sight. Note that Eq. (2) does not introduce any new free parameters. The coefficient in front of the line-of-sight velocity gradient is protected by the equivalence principle, because the galaxies should “fall” in the gravitational potential the same way as dark matter. This fact has been the rationale behind using redshift-space distortions as a cosmological probe [62].

In the context of the Ly α forest, the direct observables are absorption lines that depend on the local physics along the observer's line-of-sight. In particular, the probability of absorption depends on peculiar velocity gradients along the line of sight, making it necessary to include such terms in the expansion already in the rest frame of hydrogen clouds [7]. In EFT, this implies that the Ly α forest bias expansion has only the azimuthal symmetry w.r.t. rotations around the line-of-sight, as opposed to the galaxy distribution, which enjoys the full spherical symmetry, imposing the linear bias relation Eq. (1). In particular, in linear theory the Ly α flux fluctuations may depend now on an operator $\partial_{\parallel}^2 \Phi \propto \partial_{\parallel} v_{\parallel}^{(1)}$ (Φ stands for the Newton's potential), i.e. the linear bias relation takes the form [61, 70]

$$\delta_g^{(s)} = b_1 \delta^{(1)} + b_{\eta} \frac{\partial_{\parallel} v_{\parallel}^{(1)}}{aH}, \quad (3)$$

where b_{η} is a new bias parameter that captures the correlation of the Ly α fluctuations with projections of the dark

matter line-of-sight velocity gradient. Eq. (3) is still subject to the redshift-space mapping, which will produce an unobservable shift of b_{η} by 1.

EFT provides a systematic program for the description of non-linear effects in the Ly α forest by higher-order operators constructed from the relevant degrees of freedom, i.e. the density, velocity, and tidal fields. The structure of these operators is fixed by symmetries only, just like in Eq. (3). As such, EFT automatically implements constraints dictated by the equivalence principle for non-linear operators stemming from the redshift-space mapping [61].

We describe now the EFT for non-linear Ly α correlations in three dimensions, derived in [61]. (See also [70] for an earlier related work in the context of galaxy bias with line-of-sight selection effects.) The non-linear flux fluctuation field $\delta_F = F/\bar{F} - 1$ in redshift space at the cubic order in the linear matter overdensity $\delta^{(1)}$ is expressed as

$$\begin{aligned} \delta_F^{(s)}(\mathbf{k}) = & \sum_{n=1}^3 \left[\prod_{j=1}^n \int \frac{d^3 \mathbf{k}_j}{(2\pi)^3} \delta^{(1)}(\mathbf{k}_j) \right] K_n(\mathbf{k}_1, \dots, \mathbf{k}_n) \\ & \times (2\pi)^3 \delta_D^{(3)}(\mathbf{k} - \mathbf{k}_1 - \dots - \mathbf{k}_n), \end{aligned} \quad (4)$$

with $K_1(\mathbf{k}) = b_1 - b_{\eta} f \mu^2$ (f is the logarithmic growth factor, $\mu \equiv k_{\parallel}/k$, k_{\parallel} is the line-of-sight wavevector component), and other non-linear kernels K_n given in Supplemental Material. The EFT for Ly α features a number of free bias parameters. All together, there are two linear bias parameters, b_1 and b_{η} , and 11 non-linear bias coefficients,

$$\begin{aligned} \{b_2 &= b_{\delta^2}, b_{\mathcal{G}_2}, b_{(KK)_{\parallel}}, b_{\delta\eta}, b_{\eta^2}, b_{\Pi_{\parallel}^{[2]}}\}, \\ \{b_{\Gamma_3}, b_{\delta\Pi_{\parallel}^{[2]}}, b_{\eta\Pi_{\parallel}^{[2]}}, b_{(K\Pi^{[2]})_{\parallel}}, b_{\Pi_{\parallel}^{[3]}}\}, \end{aligned} \quad (5)$$

where the first and second lines contain coefficients of operators quadratic and cubic in linear density field, respectively. In what follows we will refer to the above bias parameters as $b_{\mathcal{O}}$, $\mathcal{O} = \delta^2, \mathcal{G}_2$ etc. Assuming that the linear density field is Gaussian-distributed with the power spectrum $P_{\text{lin}}(k)$, we obtain the 3D one-loop power spectrum

$$\begin{aligned} P_{\text{3D}}^{\text{1-loop}}(\mathbf{k} = \{k, \mu\}) = & K_1^2(\mathbf{k}) P_{\text{lin}}(k) \\ & + 2 \int_{\mathbf{q}} K_2^2(\mathbf{q}, \mathbf{k} - \mathbf{q}) P_{\text{lin}}(|\mathbf{k} - \mathbf{q}|) P_{\text{lin}}(q) \\ & + 6 K_1(\mathbf{k}) P_{\text{lin}}(k) \int_{\mathbf{q}} K_3(\mathbf{k}, -\mathbf{q}, \mathbf{q}) P_{\text{lin}}(q). \end{aligned} \quad (6)$$

We have implemented the calculation of the one-loop model above as a module in the CLASS-PT code [67]. The one-loop integrals are decomposed into powers of μ and computed using the FFTLog technique presented in [61, 73]. All together, 135 one loop integrals are computed in ≈ 1 second on one CPU core for a single point in cosmological parameter space. This speed is sufficient for Markov chain Monte Carlo (MCMC) cosmological parameter sampling. Note that sampling nuisance parameters is much faster as it does not require a re-calculation of the loop corrections.

In principle, higher derivative counterterms should be added to Eq. (6) to renormalize the loop integrals. These counterterms also capture the effects of Jeans smoothing. However, the UV-sensitivity is mild and the Jeans effects are weak at the one-loop order so that the counterterm contributions can be ignored given the current range of scales and the precision level of the SDSS data [61].

The 1D power spectrum of Ly α fluctuations measured along the line-of-sight is given by [74]

$$P_{1\text{D}}(k_{\parallel}) = \frac{1}{2\pi} \int_{k_{\parallel}}^{\infty} dk \ k P_{3\text{D}}(k, k_{\parallel}). \quad (7)$$

Importantly, the 1D power spectrum involves integration over hard momenta that are not in the perturbative regime. In EFT, one should do the above integral up to a certain cutoff k_{\max} and then add suitable counterterms that remove the cutoff dependence. As was shown in [56, 61], the leading order counterterms take the following form:

$$P_{1\text{D}}^{\text{ctr}}(k_{\parallel}) = C_0 + C_2 k_{\parallel}^2. \quad (8)$$

This increases the number of free parameters up to 13. For each point in cosmological parameter space, we compute the integral Eq. (7) numerically, assuming $k_{\max} = 3 \ h\text{Mpc}^{-1}$ as in [61].

Finally, the Ly α data from SDSS is modulated by several systematic effects. These cannot be described by EFT, and we follow the standard approach for their theoretical modeling [25], see Supplemental Material for more detail.

Analysis details. Our EFT theory involves many nuisance parameters whose redshift-dependence is not determined within the EFT itself. To estimate the impact of the EFT coefficients on parameter estimation, we run a series of Fisher matrix analyses, described in detail in

Supplemental Material. We first fix all cosmological parameters except σ_8 and study the impact of the EFT parameters. Focusing on a single redshift bin, we find that the error on σ_8 grows quickly with the number of free parameters in the fit. This is because the shape of the 1D FPS does not have enough features to break degeneracies between different EFT one-loop shapes, given the SDSS noise level. This effect can be mitigated with informative priors on the EFT parameters. We have found that we can achieve good constraints on σ_8 and maintain a significant level of flexibility if we keep the linear bias parameters $\{b_1, b_{\eta}\}$ free in the fit, while the non-linear EFT parameters are assumed to be deterministic functions of b_1 . This approach is motivated by the fact that in EFT the signal is dominated by linear fluctuations, and hence the linear bias parameters are most important to fit the data. This is the strategy that we adopt in what follows.

The non-linear bias parameters can be extracted from large sets of high-fidelity hydrodynamic simulations of 3D Ly α forest data. 3D information is crucial in order to break degeneracies between the EFT parameters that are present for 1D FPS. We extract the EFT parameters from the public power spectra measurements from the state-of-the-art public Sherwood hydrodynamic simulation [44, 59]. We will use relationships between non-linear bias parameters and b_1 , $b_{\mathcal{O}}(b_1)$, which are more robust than the bias parameter values themselves. Setting priors on bias parameters in terms of functions of b_1 also makes our analysis more flexible to possible inaccuracies in astrophysics models used in simulations. This approach is motivated by galaxy clustering analysis, where semi-analytic functions $b_{\mathcal{O}}(b_1)$ are often used in cosmological analyses, see e.g. [75–78]. In line with these arguments, we have found that the EFT parameters from the Sherwood data exhibit significant correlations with b_1 , which can be well captured with simple interpolating functions, presented in Supplemental Material. In what follows we refer to functions $b_{\mathcal{O}}(b_1)$ as “Sherwood priors.” We found that the Sherwood FPS data cannot constrain b_{Γ_3} well, so we set it to zero in all analyses following [64].

The power spectra from Sherwood simulations do not match those of SDSS for overlapping redshifts. As a result, we do not expect the Sherwood priors alone to provide a good description of the data. In order to overcome this issue we have produced mock data on 1D FPS covering the redshift range of the SDSS data using the LaCE

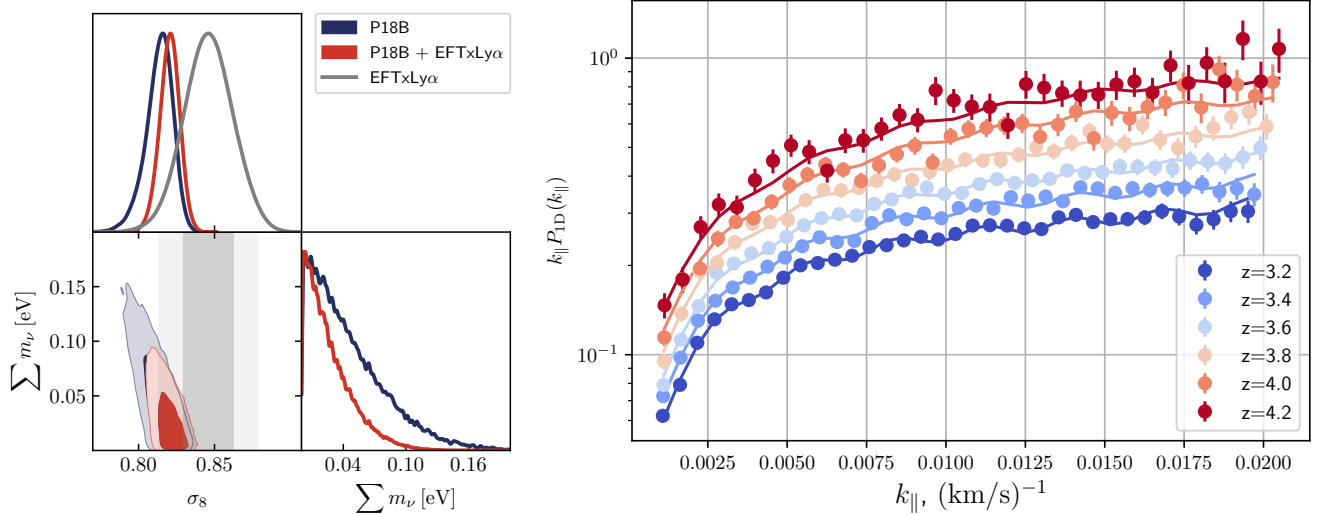


FIG. 1. *Left panel:* constraints on the mass fluctuation amplitude σ_8 from the EFT-based full-shape Ly α likelihood (EFTxLy α) presented in this work. We also display *Planck* 18 CMB + BOSS DR12 BAO (P18B) results for σ_8 and the sum of neutrino masses $\sum m_\nu$, and the results of the joint analysis of the P18B + EFTxLy α data. *Right panel:* 1-dimensional Ly α flux power spectrum data from SDSS DR14 in the range $3.1 < z < 4.3$ (central values of redshifts are quoted), along with EFT best-fit curves. Errorbars shown correspond to diagonal elements of covariance matrices with systematic weights included.

emulator [47]. The resulting synthetic spectra roughly match the real SDSS data.

Our 1D mocks do not provide 3D information needed to constrain the EFT bias parameters, but we can use them for an additional re-calibration of the 1D counterterms C_0 and C_2 that appear at the 1D level. We find that the EFT model with 3D non-linear bias parameters fixed to priors from Sherwood and 1D counterterms determined by functions $C_n(b_1)$ ($n = 0, 2$) extracted from a combination of Sherwood and LaCE simulations provides a good description of the SDSS data, as estimated based on the χ^2 statistic. Therefore, we adopt this modeling choice as our baseline. It is always possible to widen or remove some priors, which will lead to more conservative but less constraining results.

Several options are available for the description of the redshift evolution of EFT parameters. The most conservative choice is to fit the EFT parameters independently in each bin, see e.g. [64]. An alternative is to assume a smooth evolution of the free EFT parameters as a function of redshift as was done e.g. in [56]. We found that the former option works better (in terms of the χ^2 statistic), and it also provides more flexibility. This choice, which we adopt as a baseline, results in 12 free parameters for 6 redshift bins in the fit.

As far as the cosmological parameters are concerned, our Fisher matrix analysis suggests that with the above baseline settings we can obtain constraints competitive with other probes only for the mass fluctuation amplitude σ_8 , at the level of few percent. Adding other parameters to the fit leads to strong degeneracies that cannot be broken at the level of the 1D FPS data. Thus, our main analysis will have free σ_8 and other cosmological parameters fixed to a fiducial cosmology consistent with the *Planck* baseline Λ CDM model. These are $\{\omega_b, \omega_{cdm}, n_s, h, \sum m_\nu\} = \{0.02215, 0.12, 0.961, 0.678, 0\}$.

Results. To start off, we validate our pipeline on mock data generated with the LaCE emulator. Applying our pipeline to the LaCE mocks in the range $3.2 \leq z \leq 4.2$, we have found that after re-calibration of C_n , it recovers the input value of σ_8 with 0.3% accuracy, which corresponds to $\approx 15\%$ of the statistical error. This suggests that the theory systematic error of our baseline analysis is negligible.

Applying the same pipeline to the actual SDSS data we find the marginalized constraint $\sigma_8 = 0.841 \pm 0.017$ in the baseline analysis. The best-fit $\chi^2 = 170$ for 197 degrees of freedom, indicating an excellent fit to data. (Note that our covariance matrix includes diagonal systematic

weights, so the χ^2 statistic is expected to be smaller than the number of degrees of freedom.) The best-fit models and data for relevant redshift bins are shown in the right panel of Fig. 1. Using our fiducial value $\Omega_m = 0.3082$, our σ_8 constraint can be converted into a limit on $S_8 = (\Omega_m/0.3)^{1/2}\sigma_8$. We find $S_8 = 0.852 \pm 0.017$, which agrees well with the Planck CMB result 0.834 ± 0.016 [79].

Combining our EFTxLy α measurement with the *Planck* 2018 base likelihood, and adding the BAO data from BOSS DR12 as in Ref. [80], we obtain the limit on the sum of neutrino masses $\sum m_\nu < 0.080$ eV (at 95%CL), see the left panel of Fig. 1 for the 1D and 2D marginalized contours. (Other cosmological parameters of $\nu\Lambda$ CDM model were also consistently varied but not shown on the plot for compactness.) This is one of the strongest cosmological constraints on the neutrino mass to date, c.f. [63, 79–81].

Finally, we include additional cosmological parameters in our analysis. Varying both σ_8 and n_s we find a strong degeneracy between these parameters, in agreement with our Fisher matrix analysis. The data are not able to produce competitive constraints on either of these parameters individually with our baseline analysis settings. It will be interesting to see if informative priors on b_1 and b_η , or more constraining data sets, e.g. 1D FPS from DESI, could break this degeneracy.

Discussion and conclusions. We have presented the first EFT-based full-shape cosmological parameter analysis of the Ly α forest 1D clustering data from SDSS. From SDSS 1D Ly α data alone, we find a 2% constraint on the mass clustering amplitude σ_8 . Combining our likelihood with data on CMB anisotropies from *Planck* 2018 and BAO, we derive one of the strongest constraints on the total neutrino mass to date, $\sum m_\nu < 0.08$ eV. These results show the potential power of the 1D FPS when analyzed with EFT.

Our results indicate that within the EFT framework, the SDSS Ly α data are in good agreement with the baseline Planck Λ CDM cosmological model. This weakens the case for new physics interpretations of the apparent tension between Λ CDM and Ly α data in the literature. This suggests that new ingredients beyond the standard models of gas physics used in Ly α emulators may be needed to reconcile the SDSS 1D Ly α forest data with the Λ CDM.

We emphasize that our analysis should be taken in con-

junction with our assumptions about the EFT nuisance parameters. We have used priors on EFT parameters from Sherwood simulations, and priors on 1D counter-terms from the 1D power spectrum mocks produced with the LaCE emulator. These priors play a significant role in our analysis. Their removal, i.e. marginalization over EFT parameters within conservative priors, significantly degrades constraining power. Further studies of the EFT parameters with large sets of high-fidelity hydrodynamical simulations are needed in order to fully validate our priors. Similar precision measurements of EFT parameters have been previously carried out for halos and galaxies [78, 82–87]. In particular, recent studies have used informative priors on galaxy EFT parameters to improve constraints on primordial non-Gaussianity [76, 78, 87]. Performing a similar study is the main priority of the EFT program in the Ly α context. That said, we note that our model still has a significant level of flexibility as we keep linear bias parameters b_1 and b_η free for each redshift bin in our fits.

Furthermore, EFT can consistently model different Ly α measurements such as 3D Ly α autocorrelation and Ly α -quasar cross-correlation functions [88, 89], 3D power spectrum [90, 91], and cross-correlations with CMB [92]. Combining these statistics with 1D FPS can also improve our current results. For example, the degeneracy between EFT bias parameters and σ_8 can be broken by CMB lensing map and Ly α cross-correlations, and the inclusion of 3D information can alleviate the $b_1 - b_\eta$ degeneracy.

We note that our EFTxLy α approach can be readily applied to extended cosmological models, including the scenario motivated by the Hubble and S_8 tensions, see e.g. [23, 41, 93]. These, and other research directions described above, are left for future work.

Acknowledgments. We thank Andrei Cuceau, Vid Iršić, Andreu Font-Ribera, and Sokratis Trifinopoulos for useful discussions. MCMC chains produced as part of this work are generated with `Montepython` [94, 95]. This material is based upon work supported by the U.S. Department of Energy, Office of Science, Office of High Energy Physics of U.S. Department of Energy under grant Contract Number DE-SC0012567. MWT acknowledges financial support from the Simons Foundation (Grant Number 929255).

-
- [1] J. E. Gunn and B. A. Peterson, *APJ* **142**, 1633 (1965).
- [2] R. A. C. Croft, D. H. Weinberg, N. Katz, and L. Hernquist, *APJ* **488**, 532 (1997), arXiv:astro-ph/9611053 [astro-ph].
- [3] R. A. C. Croft, D. H. Weinberg, N. Katz, and L. Hernquist, *Astrophys. J.* **495**, 44 (1998), arXiv:astro-ph/9708018.
- [4] R. A. C. Croft, D. H. Weinberg, M. Bolte, S. Burles, L. Hernquist, N. Katz, D. Kirkman, and D. Tytler, *Astrophys. J.* **581**, 20 (2002), arXiv:astro-ph/0012324.
- [5] L. Hui and N. Y. Gnedin, *Mon. Not. Roy. Astron. Soc.* **292**, 27 (1997), arXiv:astro-ph/9612232.
- [6] N. Y. Gnedin and L. Hui, *Mon. Not. Roy. Astron. Soc.* **296**, 44 (1998), arXiv:astro-ph/9706219.
- [7] P. McDonald, J. Miralda-Escude, M. Rauch, W. L. W. Sargent, T. A. Barlow, R. Cen, and J. P. Ostriker, *Astrophys. J.* **543**, 1 (2000), arXiv:astro-ph/9911196.
- [8] P. McDonald *et al.* (SDSS), *Astrophys. J. Suppl.* **163**, 80 (2006), arXiv:astro-ph/0405013.
- [9] M. Viel and M. G. Haehnelt, *Mon. Not. Roy. Astron. Soc.* **365**, 231 (2006), arXiv:astro-ph/0508177.
- [10] U. Seljak, A. Slosar, and P. McDonald, *JCAP* **10**, 014 (2006), arXiv:astro-ph/0604335.
- [11] M. Viel, J. Lesgourgues, M. G. Haehnelt, S. Matarrese, and A. Riotto, *Phys. Rev. D* **71**, 063534 (2005), arXiv:astro-ph/0501562.
- [12] M. Viel, G. D. Becker, J. S. Bolton, and M. G. Haehnelt, *Phys. Rev. D* **88**, 043502 (2013), arXiv:1306.2314 [astro-ph.CO].
- [13] A. Slosar *et al.*, *JCAP* **09**, 001 (2011), arXiv:1104.5244 [astro-ph.CO].
- [14] A. Slosar *et al.*, *JCAP* **04**, 026 (2013), arXiv:1301.3459 [astro-ph.CO].
- [15] A. Boyarsky, J. Lesgourgues, O. Ruchayskiy, and M. Viel, *JCAP* **05**, 012 (2009), arXiv:0812.0010 [astro-ph].
- [16] N. Palanque-Delabrouille *et al.*, *JCAP* **1511**, 011 (2015), arXiv:1506.05976 [astro-ph.CO].
- [17] N. Palanque-Delabrouille *et al.*, *JCAP* **02**, 045 (2015), arXiv:1410.7244 [astro-ph.CO].
- [18] J. Baur, N. Palanque-Delabrouille, C. Yèche, C. Magneville, and M. Viel, *JCAP* **08**, 012 (2016), arXiv:1512.01981 [astro-ph.CO].
- [19] J. Baur, N. Palanque-Delabrouille, C. Yèche, A. Boyarsky, O. Ruchayskiy, E. Armengaud, and J. Lesgourgues, *JCAP* **12**, 013 (2017), arXiv:1706.03118 [astro-ph.CO].
- [20] V. Iršič, M. Viel, M. G. Haehnelt, J. S. Bolton, and G. D. Becker, *Phys. Rev. Lett.* **119**, 031302 (2017), arXiv:1703.04683 [astro-ph.CO].
- [21] N. Palanque-Delabrouille, C. Yèche, N. Schöneberg, J. Lesgourgues, M. Walther, S. Chabanier, and E. Armengaud, *JCAP* **04**, 038 (2020), arXiv:1911.09073 [astro-ph.CO].
- [22] A. Boyarsky, M. Drewes, T. Lasserre, S. Mertens, and O. Ruchayskiy, *Prog. Part. Nucl. Phys.* **104**, 1 (2019), arXiv:1807.07938 [hep-ph].
- [23] S. Goldstein, J. C. Hill, V. Iršič, and B. D. Sherwin, (2023), arXiv:2303.00746 [astro-ph.CO].
- [24] N. Palanque-Delabrouille *et al.* (BOSS), *Astron. Astrophys.* **559**, A85 (2013), arXiv:1306.5896 [astro-ph.CO].
- [25] S. Chabanier *et al.*, *JCAP* **07**, 017 (2019), arXiv:1812.03554 [astro-ph.CO].
- [26] H. du Mas des Bourboux *et al.* (eBOSS), *Astrophys. J.* **901**, 153 (2020), arXiv:2007.08995 [astro-ph.CO].
- [27] V. Iršič *et al.*, *Mon. Not. Roy. Astron. Soc.* **466**, 4332 (2017), arXiv:1702.01761 [astro-ph.CO].
- [28] M. Walther, J. F. Hennawi, H. Hiss, J. Oñorbe, K.-G. Lee, A. Rorai, and J. O'Meara, *Astrophys. J.* **852**, 22 (2018), arXiv:1709.07354 [astro-ph.CO].
- [29] A. Day, D. Tytler, and B. Kambalur, *Monthly Notices of the Royal Astronomical Society* **489**, 2536 (2019).
- [30] N. G. Karaçaylı *et al.*, *Mon. Not. Roy. Astron. Soc.* **509**, 2842 (2022), arXiv:2108.10870 [astro-ph.CO].
- [31] J. Vernet, H. Dekker, S. D'Odorico, L. Kaper, P. Kjaergaard, F. Hammer, S. Randich, F. Zerbi, P. J. Groot, J. Hjorth, I. Guinouard, R. Navarro, T. Adolfse, P. W. Albers, J.-P. Amans, J. J. Andersen, M. I. Andersen, P. Binetruy, P. Bristow, R. Castillo, F. Chemla, L. Christensen, P. Conconi, R. Conzelmann, J. Dam, V. de Caprio, A. de Ugarte Postigo, B. Delabre, P. di Marcaantonio, M. Downing, E. Elswijk, G. Finger, G. Fischer, H. Flores, P. Françoise, P. Goldoni, L. Guglielmi, R. Haigron, H. Hanenburg, I. Hendriks, M. Horrobin, D. Horville, N. C. Jessen, F. Kerber, L. Kern, M. Kiekebusch, P. Kleszcz, J. Klougart, J. Kragt, H. H. Larsen, J.-L. Lizon, C. Lucuix, V. Mainieri, R. Manuputy, C. Martayan, E. Mason, R. Mazzoleni, N. Michaelsen, A. Modigliani, S. Moehler, P. Møller, A. Norup Sørensen, P. Nørregaard, C. Péroux, F. Patat, E. Pena, J. Pragt, C. Reinero, F. Rigal, M. Riva, R. Roelfsema, F. Royer, G. Sacco, P. Santin, T. Schoenmaker, P. Spano, E. Sweers, R. Ter Horst, M. Tintori, N. Tromp, P. van Dael, H. van der Vliet, L. Venema, M. Vidali, J. Vinther, P. Vola, R. Winters, D. Wistisen, G. Wulterkens, and A. Zacchei, *Astronomy and Astrophysics* **536**, A105 (2011).
- [32] S. López, V. D'Odorico, S. L. Ellison, G. D. Becker,

- L. Christensen, G. Cupani, K. D. Denney, I. Páris, G. Worseck, T. A. M. Berg, S. Cristiani, M. Dessauges-Zavadsky, M. Haehnelt, F. Hamann, J. Hennawi, V. Iršič, T.-S. Kim, P. López, R. Lund Saust, B. Ménard, S. Perrotta, J. X. Prochaska, R. Sánchez-Ramírez, M. Vestergaard, M. Viel, and L. Wisotzki, *Astronomy and Astrophysics* **594**, A91 (2016).
- [33] S. S. Vogt, S. L. Allen, B. C. Bigelow, L. Bresee, W. E. Brown, T. Cantrall, A. Conrad, M. Couture, C. Delaney, H. W. Epps, D. Hilyard, D. F. Hilyard, E. Horn, N. Jern, D. Kanto, M. J. Keane, R. I. Kibrick, J. W. Lewis, J. Osborne, G. H. Pardeilhan, T. Pfister, T. Ricketts, L. B. Robinson, R. J. Stover, D. Tucker, J. M. Ward, and M. Wei, in *Instrumentation in Astronomy VIII*, Vol. 2198, edited by D. L. Crawford and E. R. Craine (SPIE, 1994) pp. 362–375.
- [34] J. M. O’Meara, N. Lehner, J. C. Howk, J. X. Prochaska, A. J. Fox, M. S. Peeples, J. Tumlinson, and B. W. O’Shea, *The Astronomical Journal* **154**, 114 (2017).
- [35] H. Dekker, S. D’Odorico, A. Kaufer, B. Delabre, and H. Kotzlowski, in *Optical and IR Telescope Instrumentation and Detectors*, Vol. 4008, edited by M. Iye and A. F. M. Moorwood (SPIE, 2000) pp. 534–545.
- [36] M. T. Murphy, G. G. Kacprzak, G. A. D. Savorgnan, and R. F. Carswell, *Mon. Not. Roy. Astron. Soc.* **482**, 3458 (2019).
- [37] N. G. Karaçaylı *et al.*, *Mon. Not. Roy. Astron. Soc.* **528**, 3941 (2024), arXiv:2306.06316 [astro-ph.CO].
- [38] C. Ravoux *et al.* (DESI), *Mon. Not. Roy. Astron. Soc.* **526**, 5118 (2023), arXiv:2306.06311 [astro-ph.CO].
- [39] K. K. Rogers and V. Poulin, (2023), arXiv:2311.16377 [astro-ph.CO].
- [40] D. C. Hooper, N. Schöneberg, R. Murgia, M. Archidiacono, J. Lesgourgues, and M. Viel, *JCAP* **10**, 032 (2022), arXiv:2206.08188 [astro-ph.CO].
- [41] A. He, R. An, M. M. Ivanov, and V. Gluscevic, (2023), arXiv:2309.03956 [astro-ph.CO].
- [42] A. Borde, N. Palanque-Delabrouille, G. Rossi, M. Viel, J. S. Bolton, C. Yèche, J.-M. LeGoff, and J. Rich, *JCAP* **07**, 005 (2014), arXiv:1401.6472 [astro-ph.CO].
- [43] G. Rossi, N. Palanque-Delabrouille, A. Borde, M. Viel, C. Yèche, J. S. Bolton, J. Rich, and J.-M. Le Goff, *Astron. Astrophys.* **567**, A79 (2014), arXiv:1401.6464 [astro-ph.CO].
- [44] J. S. Bolton, E. Puchwein, D. Sijacki, M. G. Haehnelt, T.-S. Kim, A. Meiksin, J. A. Regan, and M. Viel, *Mon. Not. Roy. Astron. Soc.* **464**, 897 (2017), arXiv:1605.03462 [astro-ph.CO].
- [45] S. Bird, K. K. Rogers, H. V. Peiris, L. Verde, A. Font-Ribera, and A. Pontzen, *JCAP* **02**, 050 (2019), arXiv:1812.04654 [astro-ph.CO].
- [46] C. Pedersen, A. Font-Ribera, T. D. Kitching, P. McDonald, S. Bird, A. Slosar, K. K. Rogers, and A. Pontzen, *JCAP* **04**, 025 (2020), arXiv:1911.09596 [astro-ph.CO].
- [47] C. Pedersen, A. Font-Ribera, K. K. Rogers, P. McDonald, H. V. Peiris, A. Pontzen, and A. Slosar, *JCAP* **05**, 033 (2021), arXiv:2011.15127 [astro-ph.CO].
- [48] M. A. Fernandez, S. Bird, and M.-F. Ho, (2023), arXiv:2309.03943 [astro-ph.CO].
- [49] D. Baumann, A. Nicolis, L. Senatore, and M. Zaldarriaga, *JCAP* **1207**, 051 (2012), arXiv:1004.2488 [astro-ph.CO].
- [50] J. J. M. Carrasco, M. P. Hertzberg, and L. Senatore, *JHEP* **09**, 082 (2012), arXiv:1206.2926 [astro-ph.CO].
- [51] V. Desjacques, D. Jeong, and F. Schmidt, *Phys. Rept.* **733**, 1 (2018), arXiv:1611.09787 [astro-ph.CO].
- [52] M. M. Ivanov, (2022), arXiv:2212.08488 [astro-ph.CO].
- [53] U. Seljak, *JCAP* **03**, 004 (2012), arXiv:1201.0594 [astro-ph.CO].
- [54] A. M. Cieplak and A. Slosar, *JCAP* **03**, 016 (2016), arXiv:1509.07875 [astro-ph.CO].
- [55] M. Garny, T. Konstandin, L. Sagunski, and S. Tulin, *JCAP* **09**, 011 (2018), arXiv:1805.12203 [astro-ph.CO].
- [56] M. Garny, T. Konstandin, L. Sagunski, and M. Viel, *JCAP* **03**, 049 (2021), arXiv:2011.03050 [astro-ph.CO].
- [57] J. J. Givans and C. M. Hirata, *Phys. Rev. D* **102**, 023515 (2020), arXiv:2002.12296 [astro-ph.CO].
- [58] S.-F. Chen, Z. Vlah, and M. White, *JCAP* **05**, 053 (2021), arXiv:2103.13498 [astro-ph.CO].
- [59] J. J. Givans, A. Font-Ribera, A. Slosar, L. Seeyave, C. Pedersen, K. K. Rogers, M. Garny, D. Blas, and V. Iršič, *JCAP* **09**, 070 (2022), arXiv:2205.00962 [astro-ph.CO].
- [60] L. Fuß and M. Garny, (2022), arXiv:2210.06117 [astro-ph.CO].
- [61] M. M. Ivanov, *Phys. Rev. D* **109**, 023507 (2024), arXiv:2309.10133 [astro-ph.CO].
- [62] S. Alam *et al.* (BOSS), *Mon. Not. Roy. Astron. Soc.* **470**, 2617 (2017), arXiv:1607.03155 [astro-ph.CO].
- [63] S. Alam *et al.* (eBOSS), *Phys. Rev. D* **103**, 083533 (2021), arXiv:2007.08991 [astro-ph.CO].
- [64] M. M. Ivanov, M. Simonović, and M. Zaldarriaga, *JCAP* **05**, 042 (2020), arXiv:1909.05277 [astro-ph.CO].
- [65] G. D’Amico, J. Gleyzes, N. Kokron, D. Markovic, L. Senatore, P. Zhang, F. Beutler, and H. Gil-Marín, (2019), arXiv:1909.05271 [astro-ph.CO].
- [66] S.-F. Chen, Z. Vlah, and M. White, *JCAP* **02**, 008 (2022), arXiv:2110.05530 [astro-ph.CO].
- [67] A. Chudaykin, M. M. Ivanov, O. H. E. Philcox, and M. Simonović, *Phys. Rev. D* **102**, 063533 (2020), arXiv:2004.10607 [astro-ph.CO].
- [68] C. Cain, E. Scannapieco, M. McQuinn, A. D’Aloisio,

- and H. Trac, arXiv e-prints , arXiv:2405.02397 (2024), arXiv:2405.02397 [astro-ph.CO].
- [69] F. Bernardeau, S. Colombi, E. Gaztanaga, and R. Scoccimarro, Phys. Rept. **367**, 1 (2002), arXiv:astro-ph/0112551 [astro-ph].
- [70] V. Desjacques, D. Jeong, and F. Schmidt, JCAP **1812**, 035 (2018), arXiv:1806.04015 [astro-ph.CO].
- [71] N. Kaiser, Mon. Not. Roy. Astron. Soc. **227**, 1 (1987).
- [72] R. Scoccimarro, Phys. Rev. **D70**, 083007 (2004), arXiv:astro-ph/0407214 [astro-ph].
- [73] M. Simonovic, T. Baldauf, M. Zaldarriaga, J. J. Carrasco, and J. A. Kollmeier, JCAP **1804**, 030 (2018), arXiv:1708.08130 [astro-ph.CO].
- [74] S. L. Lumsden, A. F. Heavens, and J. A. Peacock, MNRAS **238**, 293 (1989).
- [75] F. Beutler *et al.* (BOSS), Mon. Not. Roy. Astron. Soc. **466**, 2242 (2017), arXiv:1607.03150 [astro-ph.CO].
- [76] G. Cabass, M. M. Ivanov, O. H. E. Philcox, M. Simonovic, and M. Zaldarriaga, (2022), arXiv:2211.14899 [astro-ph.CO].
- [77] G. Cabass, M. M. Ivanov, O. H. E. Philcox, M. Simonović, and M. Zaldarriaga, (2022), arXiv:2204.01781 [astro-ph.CO].
- [78] M. M. Ivanov, C. Cuesta-Lazaro, S. Mishra-Sharma, A. Obuljen, and M. W. Toomey, (2024), arXiv:2402.13310 [astro-ph.CO].
- [79] N. Aghanim *et al.* (Planck), (2018), arXiv:1807.06209 [astro-ph.CO].
- [80] M. M. Ivanov, M. Simonović, and M. Zaldarriaga, Phys. Rev. D **101**, 083504 (2020), arXiv:1912.08208 [astro-ph.CO].
- [81] A. G. Adame *et al.* (DESI), (2024), arXiv:2404.03002 [astro-ph.CO].
- [82] T. Lazeyras and F. Schmidt, JCAP **1809**, 008 (2018), arXiv:1712.07531 [astro-ph.CO].
- [83] M. M. Abidi and T. Baldauf, JCAP **1807**, 029 (2018), arXiv:1802.07622 [astro-ph.CO].
- [84] A. Barreira, JCAP **12**, 031 (2020), arXiv:2009.06622 [astro-ph.CO].
- [85] A. Barreira, T. Lazeyras, and F. Schmidt, (2021), arXiv:2105.02876 [astro-ph.CO].
- [86] T. Lazeyras, A. Barreira, and F. Schmidt, JCAP **10**, 063 (2021), arXiv:2106.14713 [astro-ph.CO].
- [87] G. Cabass, O. H. E. Philcox, M. M. Ivanov, K. Akitsu, S.-F. Chen, M. Simonović, and M. Zaldarriaga, (2024), arXiv:2404.01894 [astro-ph.CO].
- [88] H. du Mas des Bourboux *et al.*, Astrophys. J. **901**, 153 (2020), arXiv:2007.08995 [astro-ph.CO].
- [89] DESI Collaboration, A. G. Adame, J. Aguilar, S. Ahlen, S. Alam, D. M. Alexander, M. Alvarez, O. Alves, A. Anand, U. Andrade, E. Armengaud, S. Avila, A. Aviles, H. Awan, S. Bailey, C. Baltay, A. Bault, J. Bautista, J. Behera, S. BenZvi, F. Beutler, D. Bianchi, C. Blake, R. Blum, S. Brieden, A. Brodzeller, D. Brooks, E. Buckley-Geer, E. Burtin, R. Calderon, R. Canning, A. C. Rosell, R. Cereskaite, J. L. Cervantes-Cota, S. Chabanier, E. Chaussidon, J. Chaves-Montero, S. Chen, X. Chen, T. Claybaugh, S. Cole, A. Cuceu, T. M. Davis, K. Dawson, R. de la Cruz, A. de la Macorra, A. de Mattia, N. Deiosso, A. Dey, B. Dey, J. Ding, Z. Ding, P. Doel, J. Edelstein, S. Eftekharzadeh, D. J. Eisenstein, A. Elliott, P. Fagrelius, K. Fanning, S. Ferraro, J. Ereza, N. Findlay, B. Flaugher, A. Font-Ribera, D. Forero-Sánchez, J. E. Forero-Romero, C. García-Quintero, E. Gaztañaga, H. Gil-Marín, S. G. A. Gontcho, A. X. Gonzalez-Morales, V. Gonzalez-Perez, C. Gordon, D. Green, D. Gruen, R. Gsponer, G. Gutierrez, J. Guy, B. Hadzhiyska, C. Hahn, M. M. S. Hanif, H. K. Herrera-Alcantar, K. Honscheid, C. Howlett, D. Huterer, V. Iršić, M. Ishak, S. Juneau, N. G. Karacayli, R. Kehoe, S. Kent, D. Kirkby, A. Kremin, A. Krolewski, Y. Lai, T. W. Lan, M. Landriau, D. Lang, J. Lasker, J. M. L. Goff, L. L. Guillou, A. Leauthaud, M. E. Levi, T. S. Li, E. Linder, K. Lodha, C. Magneville, M. Manera, D. Margala, P. Martini, M. Maus, P. McDonald, L. Medina-Varela, A. Meisner, J. Mena-Fernández, R. Miquel, J. Moon, S. Moore, J. Moustakas, N. Mudur, E. Mueller, A. Muñoz-Gutiérrez, A. D. Myers, S. Nadathur, L. Napolitano, R. Neveux, J. A. Newman, N. M. Nguyen, J. Nie, G. Niz, H. E. Noriega, N. Padmanabhan, E. Paillas, N. Palanque-Delabrouille, J. Pan, S. Penmetsa, W. J. Percival, M. Pieri, M. Pinon, C. Poppett, A. Porredon, F. Prada, A. Pérez-Fernández, I. Pérez-Ràfols, D. Rabinowitz, A. Raichoor, C. Ramírez-Pérez, S. Ramirez-Solano, M. Rashkovetskyi, C. Ravoux, M. Rezaie, J. Rich, A. Rocher, C. Rockosi, N. A. Roe, A. Rosado-Marin, A. J. Ross, G. Rossi, R. Ruggieri, V. Ruhlmann-Kleider, L. Samushia, E. Sanchez, C. Saulder, E. F. Schlaflly, D. Schlegel, M. Schubnell, H. Seo, R. Sharples, J. Silber, F. Sinigaglia, A. Slosar, A. Smith, D. Sprayberry, T. Tan, G. Tarlé, S. Trusov, R. Vaisakh, D. Valcin, F. Valdes, M. Vargas-Magaña, L. Verde, M. Walther, B. Wang, M. S. Wang, B. A. Weaver, N. Weaverdyck, R. H. Wechsler, D. H. Weinberg, M. White, J. Yu, Y. Yu, S. Yuan, C. Yèche, E. A. Zaborowski, P. Zarrouk, H. Zhang, C. Zhao, R. Zhao, R. Zhou, and H. Zou, arXiv e-prints , arXiv:2404.03001 (2024), arXiv:2404.03001 [astro-ph.CO].
- [90] M. L. Abdul-Karim, E. Armengaud, G. Mention, S. Chabanier, C. Ravoux, and Z. Lukic, arXiv e-prints , arXiv:2310.09116 (2023), arXiv:2310.09116 [astro-ph.CO].

-
- [91] R. de Belsunce, O. H. E. Philcox, V. Irsic, P. McDonald, J. Guy, and N. Palanque-Delabrouille, arXiv e-prints , arXiv:2403.08241 (2024), arXiv:2403.08241 [astro-ph.CO].
- [92] C. Doux, E. Schaan, E. Aubourg, K. Ganga, K.-G. Lee, D. N. Spergel, and J. Tréguer, Phys. Rev. D **94**, 103506 (2021).
- [93] E. Abdalla *et al.*, JHEAp **34**, 49 (2022), arXiv:2203.06142 [astro-ph.CO].
- [94] B. Audren, J. Lesgourges, K. Benabed, and S. Prunet, JCAP **1302**, 001 (2013), arXiv:1210.7183 [astro-ph.CO].
- [95] T. Brinckmann and J. Lesgourges, Phys. Dark Univ. **24**, 100260 (2019), arXiv:1804.07261 [astro-ph.CO].

Supplemental Material

1. ANALYSIS DETAILS

Perturbation theory kernels. We start with the perturbation theory kernels for Ly α ,

$$\begin{aligned} K_1(\mathbf{k}) &= b_1 - b_\eta f \mu^2, \\ K_2(\mathbf{k}_1, \mathbf{k}_2) &= \frac{b_2}{2} + b_{G_2} \left(\frac{(\mathbf{k}_1 \cdot \mathbf{k}_2)^2}{k_1^2 k_2^2} - 1 \right) + b_1 F_2(\mathbf{k}_1, \mathbf{k}_2) - b_\eta f \mu^2 G_2(\mathbf{k}_1, \mathbf{k}_2) - f b_{\delta\eta} \frac{\mu_2^2 + \mu_1^2}{2} + b_{\eta^2} f^2 \mu_1^2 \mu_2^2 \\ &\quad + b_1 f \frac{\mu_1 \mu_2}{2} \left(\frac{k_2}{k_1} + \frac{k_1}{k_2} \right) - b_\eta f^2 \frac{\mu_1 \mu_2}{2} \left(\frac{k_2}{k_1} \mu_2^2 + \frac{k_1}{k_2} \mu_1^2 \right) + b_{(KK)_\parallel} \left(\mu_1 \mu_2 \frac{(\mathbf{k}_1 \cdot \mathbf{k}_2)}{k_1 k_2} - \frac{\mu_1^2 + \mu_2^2}{3} + \frac{1}{9} \right) \\ &\quad + b_{\Pi_\parallel^{(2)}} \left(\mu_1 \mu_2 \frac{(\mathbf{k}_1 \cdot \mathbf{k}_2)}{k_1 k_2} + \frac{5}{7} \mu^2 \left(1 - \frac{(\mathbf{k}_1 \cdot \mathbf{k}_2)^2}{k_1^2 k_2^2} \right) \right), \end{aligned} \tag{S1}$$

with $\mu_i = (\hat{\mathbf{z}} \cdot \hat{\mathbf{k}}_i)$, $\hat{\mathbf{z}}$ denoting the line-of-sight direction unit vector, $f = d \ln D_+ / d \ln a$ (D_+ is the growth factor), and we have used the usual density and velocity kernels from standard cosmological perturbation theory:

$$\begin{aligned} F_2(\mathbf{k}_1, \mathbf{k}_2) &= \frac{5}{7} + \frac{2}{7} \frac{(\mathbf{k}_1 \cdot \mathbf{k}_2)^2}{k_1^2 k_2^2} + \frac{1}{2} \frac{\mathbf{k}_1 \cdot \mathbf{k}_2}{k_1 k_2} \left(\frac{k_1}{k_2} + \frac{k_2}{k_1} \right), \\ G_2(\mathbf{k}_1, \mathbf{k}_2) &= \frac{3}{7} + \frac{4}{7} \frac{(\mathbf{k}_1 \cdot \mathbf{k}_2)^2}{k_1^2 k_2^2} + \frac{1}{2} \frac{\mathbf{k}_1 \cdot \mathbf{k}_2}{k_1 k_2} \left(\frac{k_1}{k_2} + \frac{k_2}{k_1} \right), \end{aligned} \tag{S2}$$

The general expression for the K_3 kernel is quite cumbersome. Below we present it only for the kinematic configurations that appear in the one-loop power spectrum integrals:

$$\begin{aligned}
& \int_{\mathbf{q}} K_3(\mathbf{k}, \mathbf{q}, -\mathbf{q}) P_{\text{lin}}(q) \\
&= b_1 \int_{\mathbf{q}} F_3(\mathbf{k}, \mathbf{q}, -\mathbf{q}) P_{\text{lin}}(q) - f b_\eta \mu^2 \int_{\mathbf{q}} G_3(\mathbf{q}, -\mathbf{q}, \mathbf{k}) P_{\text{lin}}(q) \\
&\quad + \int_{\mathbf{q}} \left[1 - (\hat{\mathbf{k}} \cdot \hat{\mathbf{q}})^2 \right] P_{\text{lin}}(q) \\
&\quad \times \left\{ \frac{4}{21} (5b_{G_2} + 2b_{\Gamma_3}) \left[\left(\frac{(\mathbf{k} - \mathbf{q}) \cdot \mathbf{q}}{|\mathbf{k} - \mathbf{q}| q} \right)^2 - 1 \right] - \frac{2}{21} f b_{\delta\eta} \left[\frac{3(k_{\parallel} - q_{\parallel})^2}{|\mathbf{k} - \mathbf{q}|^2} + \frac{5q_{\parallel}^2}{q^2} \right] \right. \\
&\quad + \frac{4}{7} f^2 b_{\eta^2} \frac{q_{\parallel}^2 (k_{\parallel} - q_{\parallel})^2}{q^2 |\mathbf{k} - \mathbf{q}|^2} + \frac{20}{21} b_{(KK)}{}_{\parallel} \left[\frac{(\mathbf{k} \cdot \mathbf{q} - q^2)(k_{\parallel} - q_{\parallel})q_{\parallel}}{|\mathbf{k} - \mathbf{q}|^2 q^2} - \frac{1}{3} \frac{(k_{\parallel} - q_{\parallel})^2}{|\mathbf{k} - \mathbf{q}|^2} - \frac{1}{3} \frac{q_{\parallel}^2}{q^2} + \frac{1}{9} \right] \\
&\quad + \frac{10}{21} b_{\Pi_{\parallel}^{[2]}} \frac{(\mathbf{k} \cdot \mathbf{q} - q^2)}{|\mathbf{k} - \mathbf{q}|^2} \frac{(k_{\parallel} - q_{\parallel})^2}{q^2} + \frac{10}{21} \left[b_{\delta\Pi_{\parallel}^{[2]}} - \frac{1}{3} b_{(K\Pi_{\parallel}^{[2]})} - f b_{\eta\Pi_{\parallel}^{[2]}} \frac{q_{\parallel}^2}{q^2} \right] \frac{(k_{\parallel} - q_{\parallel})^2}{|\mathbf{k} - \mathbf{q}|^2} \\
&\quad + \frac{10}{21} b_{(K\Pi_{\parallel}^{[2]})} \frac{(\mathbf{q} \cdot \mathbf{k} - q^2)}{q |\mathbf{k} - \mathbf{q}|} \frac{q_{\parallel}(k_{\parallel} - q_{\parallel})}{q |\mathbf{k} - \mathbf{q}|} + \frac{10}{21} f b_{\Pi_{\parallel}^{[2]}} \frac{q_{\parallel}(k_{\parallel} - q_{\parallel})^3}{q^2 |\mathbf{k} - \mathbf{q}|^2} \\
&\quad + (b_{\Pi_{\parallel}^{[3]}} + 2b_{\Pi_{\parallel}^{[2]}}) \left[\frac{13}{21} \frac{\mathbf{k} \cdot \mathbf{q} - q^2}{|\mathbf{k} - \mathbf{q}|^2} \frac{q_{\parallel}(k_{\parallel} - q_{\parallel})}{q^2} - \frac{5\mu^2}{9} \left[\left(\frac{(\mathbf{k} - \mathbf{q}) \cdot \mathbf{q}}{|\mathbf{k} - \mathbf{q}| q} \right)^2 - \frac{1}{3} \right] \right] \\
&\quad \left. + \frac{2}{21} f b_1 \left[5 \frac{q_{\parallel}(k_{\parallel} - q_{\parallel})}{q^2} + 3 \frac{q_{\parallel}(k_{\parallel} - q_{\parallel})}{|\mathbf{k} - \mathbf{q}|^2} \right] - \frac{2}{7} f^2 b_\eta \frac{q_{\parallel}(k_{\parallel} - q_{\parallel})}{q^2 |\mathbf{k} - \mathbf{q}|^2} [(k_{\parallel} - q_{\parallel})^2 + q_{\parallel}^2] \right\}. \tag{S3}
\end{aligned}$$

The expressions for the standard fluid kernels F_3 and G_3 can be found e.g. in [S69].

Treatment of Systematics. We model the SiIII oscillations as a multiplicative factor [S8, S24]

$$\kappa_{\text{SiIII}} = 1 + 2 \left(\frac{f_{\text{SiIII}}}{1 - \bar{F}_{\text{fid}}} \right) \cos(v k_{\parallel}) + \left(\frac{f_{\text{SiIII}}}{1 - \bar{F}_{\text{fid}}} \right)^2, \tag{S4}$$

with $f_{\text{SiIII}} = 8.7 \cdot 10^{-3}$, $v = 2\pi/(0.0028)$ km/s, $\bar{F}_{\text{fid}} = e^{-0.0025(1+z)^{3.7}}$. Thermal broadening is modeled with the damping kernel $e^{-(k_{\parallel}/k_s)^2}$ with $k_s = 0.11(\text{km/s})^{-1}$. We note that our main results are insensitive to these particular choices, i.e. we find similar constraints when the parameters describing the above systematic effects are varied.

Fisher matrix analysis. We now present details of the Fisher matrix analysis that we use to determine the baseline parameters of our likelihood analysis. We focus on a single redshift of the data, centered at $z = 3.2$. Our analysis shows that the error on σ_8 grows fast with a number of free parameters in the fit, see Fig. S1. In particular, the data loose sensitivity to σ_8 almost entirely if non-linear bias parameters are varied. We motivates a strategy to keep the linear bias parameters free, and fix the non-linear ones to values informed by simulations. Note that even in this case we find a very significant degeneracy between σ_8 , b_1 and b_η , see the right panel of Fig. S1.

As far as the cosmological parameters are concerned, our Fisher matrix analysis suggests that with the above baseline settings we can obtain constraints competitive with other probes only for the mass fluctuation amplitude σ_8 , at the level of few percent. Specifically, focusing on one redshift, we find that adding n_s to the fit yield constraints $\{\frac{\sigma_{\sigma_8}}{\sigma_8}, \sigma_{n_s}\} = \{0.25, 0.06\}$; while adding to the fit ω_{cdm} produces uninformative constraints $\{\frac{\sigma_{\sigma_8}}{\sigma_8}, \sigma_{n_s}, \frac{\sigma_{\omega_{\text{cdm}}}}{\omega_{\text{cdm}}}\} = \{0.67, 0.28, 0.52\}$. In addition, the cosmological parameter contours are extremely degenerate, e. g. for the analysis with free n_s and σ_8 we find a correlation coefficient -0.99 , which indicates that measuring these parameters individually with the current EFT settings is challenging. We have confirmed this statement in a full MCMC analysis as well. Better priors on b_1 and b_η from hydrodynamical simulations will be needed in order to measure n_s and σ_8 individually from the 1D FPS.

EFT bias parameters from the Sherwood simulations. We fit the public 3D power spectra of Ly α fluctuations from the Sherwood simulations using the same methodology as in [S61]. The public data cover four redshift bins with

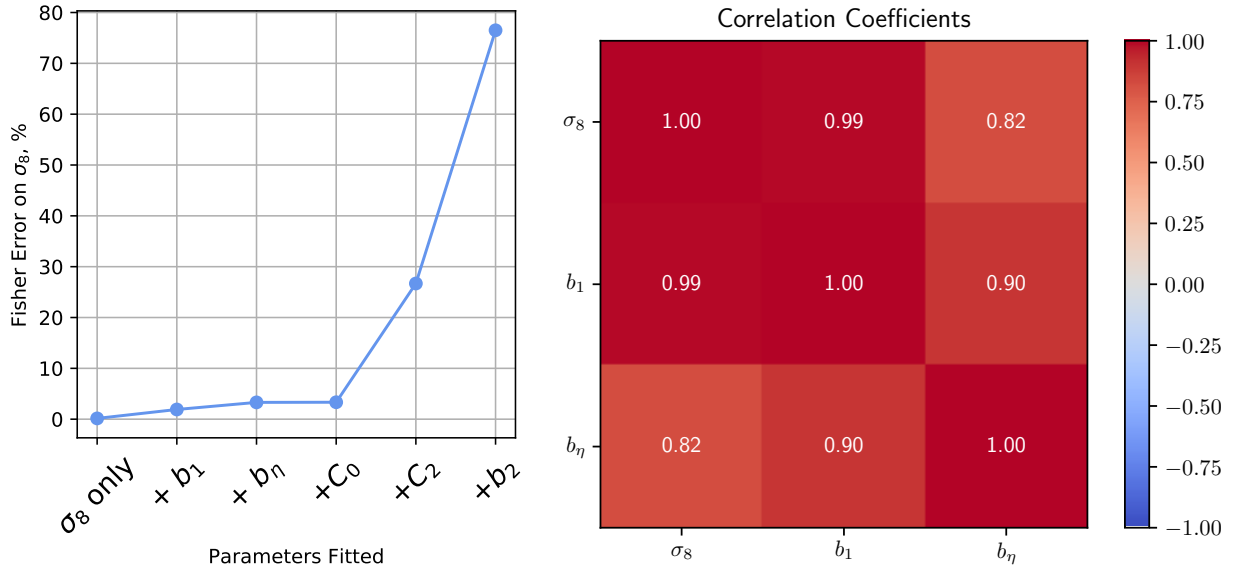


FIG. S1. *Left panel:* Marginalized Fisher errors on the mass fluctuation amplitude σ_8 as a function of a number of free EFT parameters in the fit. Results are reported for a single redshift bin $3.1 < z < 3.3$. *Right panel:* Fisher correlation coefficients for a fit with only three parameters: σ_8, b_1, b_η .

centers at $z = [2, 2.4, 2.8, 3.2]$. The $z = 2.8$ and $z = 3.2$ data were fitted before in [S61]. For the remaining two redshifts, we use the parameter drift plots to estimate the data cut k_{\max} for which the EFT model is applicable. Our measurements of different nonlinear bias parameters $b_{\mathcal{O}}$ versus corresponding values of b_1 are presented in Fig. S2, along with the linear fits to the data points. Error bars on the quadratic parameters follow from the Gaussian covariance for the power spectrum. The errors on the EFT parameters depend very strongly on k_{\max} used in the fits, and the possible choices of k_{\max} are limited by the binning of the public Sherwood power spectra. Because of these reasons, for some cubic bias parameters the nominal errorbars appear to be quite small, which may bias the $b_{\mathcal{O}}(b_1)$ relations extracted from the simulation. In order to be conservative and avoid overfitting, we assume a flat error 1 on all cubic bias parameters. Finally, we also assume flat errors 1 on $C_0/(5 \cdot 10^{-3} [h^{-1}\text{Mpc}])$ and $C_2/(5 \cdot 10^{-4} [h^{-1}\text{Mpc}]^3)$, because the covariance for the 1D FPS of Sherwood is not available, so there is no reliable way to estimate the errors in this case. We found that the dependencies $b_{\mathcal{O}}(b_1)$ and $C_n(b_1)$ can be well fitted with linear functions,

$$b_{\mathcal{O}} = A_{\mathcal{O}} b_1 + B_{\mathcal{O}}. \quad (\text{S5})$$

The best-fit values of $A_{\mathcal{O}}$ and $B_{\mathcal{O}}$ are given in Table I. For C_n we have

$$\frac{C_0}{[h^{-1}\text{Mpc}]} = -0.17b_1 - 0.0148, \quad \frac{C_2}{[h^{-1}\text{Mpc}]^3} = -9.7 \cdot 10^{-4}b_1 + 9.4 \cdot 10^{-5}. \quad (\text{S6})$$

Operator \mathcal{O}	\mathcal{G}_2	δ^2	η^2	$\delta\eta$	$(KK)_{\parallel}$	$\Pi_{\parallel}^{[2]}$	$\Pi_{\parallel}^{[3]}$	$\delta\Pi_{\parallel}^{[2]}$	$(K\Pi^{[2]})_{\parallel}$	$\eta\Pi_{\parallel}^{[2]}$
$A_{\mathcal{O}}$	0.089	-0.32	-2.0	4.4	0.45	2.2	-7.0	8.2	7.8	-9.9
$B_{\mathcal{O}}$	-0.18	-0.52	0.19	0.063	-0.14	-0.074	0.0043	-1.5	-0.79	-2.0

TABLE I. Numerical values for the fit to the Sherwood EFT parameters as functions of the linear bias b_1 .

Synthetic 1D FPS data from LaCE. We use the Cabayol23 neural network emulator available from LaCE¹ to generate

¹ <https://github.com/igmhub/LaCE/tree/main>

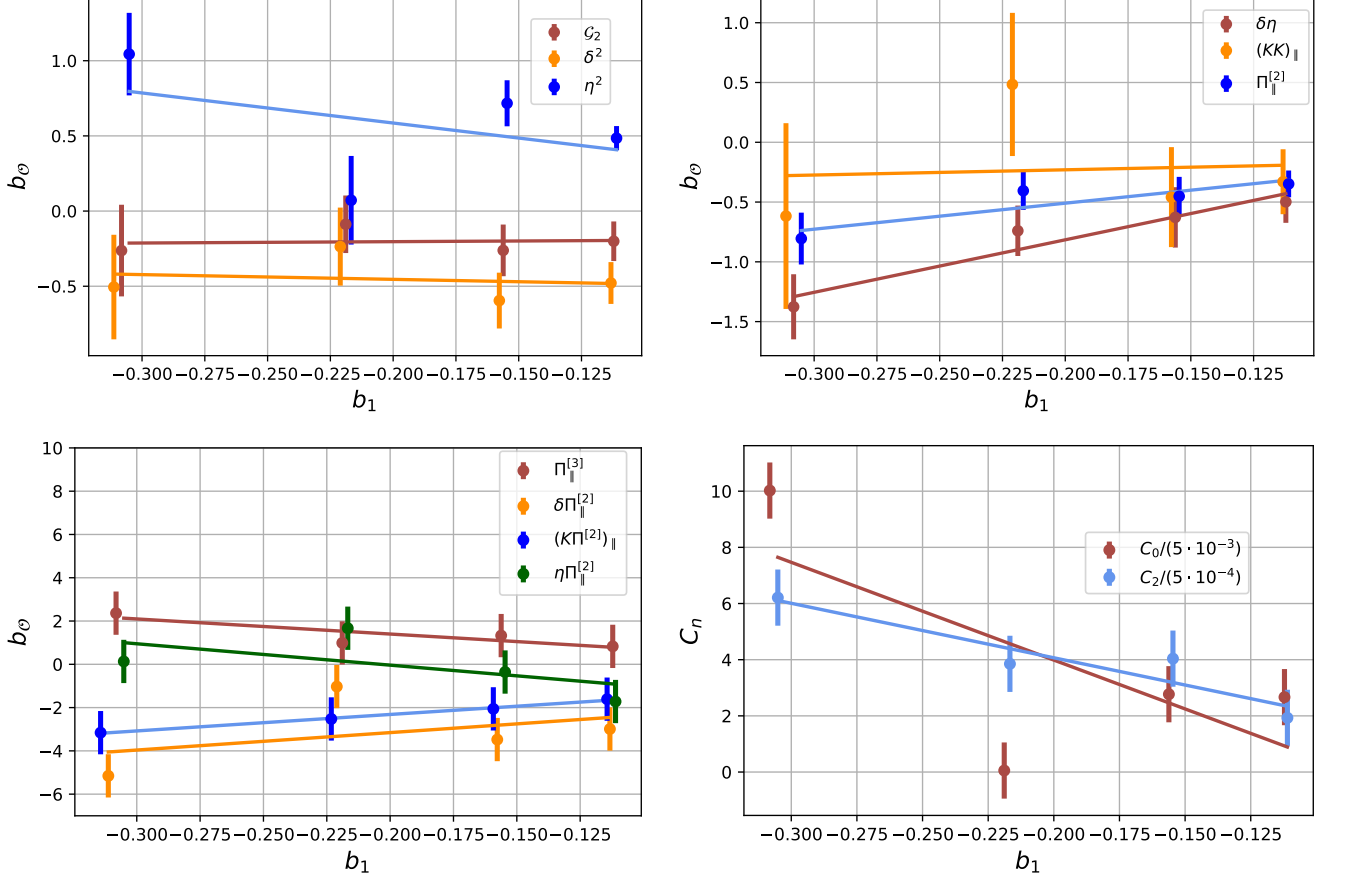


FIG. S2. Bias parameters and counterterterms of the Sherwood simulation data. Solid lines depict the linear fits to the data.

1-dimensional Ly α power spectrum where we vary only σ_T and γ and scanning over a range from {0.0,0.5} and {0.5,2.0} respectively. The typical fits to FPS at a single redshift has a reduced χ^2 ranging from ~ 1.2 to 1.4 which indicates a reasonable match, but not a good fit. We find that the last point largely arises due to discrepancies at smaller scales as can be appreciated from the r.h.s. of Fig. 1. Note that we have not optimized the full set of the LaCE parameters to precisely reproduce the data. This is done in order to avoid double counting of information when we use the LaCE mocks for re-calibration of 1D EFT counterterms. The best-fit C_n parameters extracted from our mocks are:

$$\frac{C_0}{[h^{-1}\text{Mpc}]} = -0.17b_1 - 0.2053, \quad \frac{C_2}{[h^{-1}\text{Mpc}]^3} = -9.7 \cdot 10^{-4}b_1 + 2.16 \cdot 10^{-2}. \quad (\text{S7})$$

We see that the typical momentum scales associated with these parameters are around $4 h\text{Mpc}^{-1}$, which is consistent with the EFT expectation that they should be of the order of $k_{\text{NL}} \sim (5 - 10) h\text{Mpc}^{-1}$.